Proton Conduction Inhibited by Xe Hydrates in the Water Nanotube of the Molecular Porous Crystal {{[RuIII(H2bim)3](TMA)}2 mH2O}n

doi: 10.1021/acs.jpcc.9b05779

Proton Conduction Inhibited by Xe Hydrates in the Water Nanotube of Molecular Porous Crystal $\{\{[Ru^{III}(H_2bim)_3](TMA)\}_2 \cdot mH_2O\}_n$

Hiroshi Matsui, [*,†] Tomotaka Sasaki, [†] and Makoto Tadokoro[‡,§]

[†]Department of Physics, Graduate School of Science, Tohoku University, Sendai 980-8578, Japan

[‡]Department of Chemistry, Faculty of Science, and [§]Research Institute for Science and Technology, Tokyo University of Science, Tokyo 162-8601, Japan

[*]E-mail: hiroshi.matsui.b2@tohoku.ac.jp

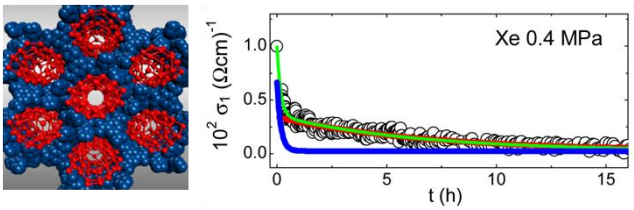

ABSTRACT:

Gas sorption and molecular (ionic) storages are important functionalities in porous materials. In molecular porous crystal $\{\{[Ru^{III}(H_2bim)_3](TMA)\}_2 \cdot mH_2O\}_n$, the hydrophilic nanochannel accommodates the water nanotube (WNT) composed of a $4^4 6^{10} 7^4$-polyhedral cage. The experiment on weight change reveals that the cage structure is maintained above 50%RH (relative humidity) at 294 K. As the relative humidity is reduced from 80 to 50%RH, the proton conductivity exponentially decreases from 0.02 to 0.01 $(\Omega cm)^{-1}$ owing to the dehydration of inner H_2O molecules through WNT, which acts as a nanofluidic channel.

Upon pressurizing Xe at 0.4 MPa for 50%RH, the proton conductivity exponentially decreases and approaches to 0 $(\Omega cm)^{-1}$. The infrared and ^{129}Xe-NMR experiments make clear that Xe together with about 25H_2O molecules per cage is stabilized in WNT at low pressures compared to Xe-clathrate hydrate. Those results experimentally demonstrate that the Xe hydrate inhibits the proton conduction. The formation of Xe hydrate is characterized by fast and slow processes with the translational diffusion constant of 1 x 10^{-10} and 6 x 10^{-12} m^2/s, respectively. The reorganization and hardening of the hydrogen-bonding water network are considered to diminish the conducting pass of proton, and to reduce the protonic transfer from H_3O^+ to adjacent H_2O.

1. INTRODUCTION

Confined water in porous and biological materials has interdisciplinary research interest to explore applications such as novel fuel-cell electrolytes,[1] desalination,[2,3] bioprotonic and nanofluidic devices.[4-12] Many studies on confined water have been performed in a variety of nanospaces like carbon nanotubes,[13-16] membranes,[17] metal-organic frameworks,[18-20] and molecular porous crystals involving a water nanotube[21,22] or water chain.[23] Moreover, those nanospaces have been actively utilized for the arrangements and storages of molecules or ions.[24-26]

Lots of hydrophobic gas molecules are stabilized in the form of clathrate hydrate at high pressures and low temperatures.[27] A methane hydrate reserved under deep sea is representative and valuable as new energy resources. In particular, a clathrate hydrate of Xe is made at room temperature above 1 MPa.[28] Therefore we expect that Xe is suitable for examining an absorption process and influence to proton conduction in nanochannel water.

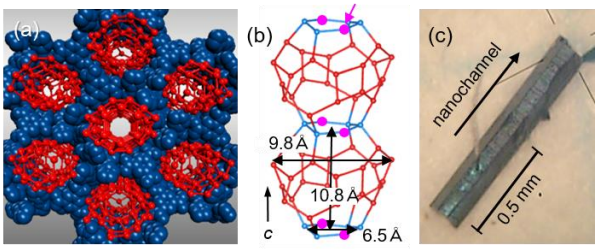

Figure 1. (a) Perspective view of WNT (red circles and lines) surrounded by the insulating framework molecules (navy blue circles). (b) Cage structure of WNT in the hydrophilic nanochannel. The lines and circles denote hydrogen bonds and oxygen atoms of H_2O, respectively. (c) Green-colored single crystal with a needle shape.

Xe holds a paramount effect as inhalation anesthesia. Various substances are known to cause general anesthesia, whereas the anesthetic mechanism has not been established so far.[29,30] More than half a century ago, Linus Pauling has proposed that a hydrate microcrystal of Xe increases an impedance of nervous systems and leads human unconsciousness.[31] A proton is well known to play physiological roles, and to carry electric signals in biological systems like bacteriorhodopsin.[32] If it is experimentally proved that a Xe hydrate makes an influence to proton conduction with nanochannel water, we might approach a probable mechanism of anesthesia. In this study, we aim to understand the diffusion process of H_2O and Xe molecules, and to explore the influence of Xe hydrates to the proton conduction in the water nanotube (WNT) of molecular porous crystal $\{\{[Ru^{III}(H_2bim)_3](TMA)\}_2 \cdot mH_2O\}_n$.[33] Thanks to the large single crystals with millimeter size, several experimental methods were successfully carried out.

In the melting state above 219 K, WNT is regarded as a liquid-like dynamic water cluster in the insulating nanochannel of molecular porous crystal (Figure 1(a)),[33,34] which has a structure network of three-dimensional (10.3)-*b* net[35] formed by complementary hydrogen bonds between $[Ru^{III}(H_2bim)_3]^{3+}$ (tris-biimidazole Ru^{3+} complex) and TMA^{3-} (trimesate). The oxygen position of WNT is determined by the X-ray crystal structure analysis, while the inner H_2O is hardly identified owing to large thermal fluctuations at room temperature. The WNT consists of $4^4 6^{10} 7^4$-polyhedral cages that are aligned along *c*. Two cages ($60H_2O$) are shown in Figure 1(b). The single cage ($30H_2O$) is classified into four hydration shells. The primary and secondary hydration shells (red circles) are composed of $24H_2O$ molecules hydrogen bonded to the carboxylate (COO^- group) of TMA^{3-}, and then WNT is strongly constrained in addition to the interfacial interaction from the framework.[22] The residual $6H_2O$ molecules in the form of cyclic hexagon belong to the tertiary hydration shell (blue circles), and the fourth one possessing a free

OH (pink circles). The green-colored single crystal with needle shape has typical lengths of 0.5-1.5 mm and widths of 0.1-0.5 mm (Figure 1(c)).

2. EXPERIMENTAL METHODS

2.1. Sample preparation

The starting material is the molecular porous crystal $\{\{[Ru^{III}(H_2bim)_3](TMA)\}_2 \cdot 30H_2O \cdot 3THF\}_n$. The structure and synthesis were already reported by M. Tadokoro *et al.*[33] Here THF denotes a tetrahydrofuran, three of which reside in the single cage of WNT. The crystal sealed in a vessel is dried for an hour in the environment of 55%RH. The THF is selectively removed from WNT, and we obtain the single crystal $\{\{[Ru^{III}(H_2bim)_3](TMA)\}_2 \cdot 30H_2O\}_n$. As the crystal is immersed in pure water, the inner water molecules are embedded without changing the structure of WNT and nanochannel framework.

2.2 Measurement of sample weight

A weight change of single crystal is measured at 1 atm with a commercial thermogravimetry (TG) apparatus in combination with a humid controlling system (Brucker AXS, TG-DTA2000SA/HC9700, Germany). For each target relative humidity at 0-90%RH, the sample was kept for 24 h to achieve an equilibrium, and then we measured the sample weight. From the weight change, we evaluated the amount of water molecules per cage length in the single nanochannel.

2.3 Microwave conductivity measurement

Microwave conductivity is measured with our homemade system (Figure 2) on the basis of

cavity perturbation technique,[36] the advantage of which is unnecessary to connect any electrical leads to a sample. A cylindrical cavity made of oxygen free copper resonates at 16.2 GHz for TE_{011} mode, and the Q value is about 18,000. In Figure 2, magnetic-field components are not shown. A single-crystal sample is mounted on the top of thin quartz rod (0.5 mm in diameter), where the maximum ac-electric field is applied parallel to the nanochannel. Inside the cavity, relative humidity (20-80%RH) is adjustable with a circulation-type humid controlling system (KTC-Z02A-S, Kotohira, Japan), and Xe partial pressure is applicable up to 0.4 MPa.

Employing a microwave generator, frequencies are swept in the vicinity of resonance frequency of the cavity. The incident microwave propagating through a coaxial cable enters and resonates in the cavity. The power of transmitted wave is detected by a power meter. From a Lorentzian-type resonance curve, we obtain a resonance frequency (f) and width (W) for the cases with (s) and without a sample (0) in the cavity. From the difference of resonance frequency

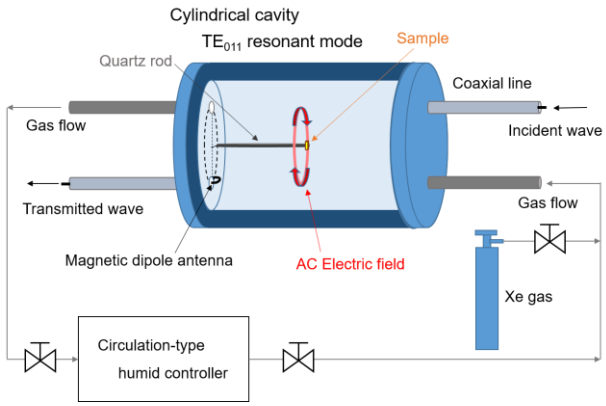

Figure 2. Measuring system of microwave conductivity based on cavity perturbation technique. We are available to control relative humidity and Xe pressure in the cylindrical cavity. A small single-crystal sample is positioned at the maximum ac-electric field.

($\Delta f = f_s - f_0$) and width ($\Delta W = W_s - W_0$), we are available to calculate a complex dielectric constant ($\varepsilon = \varepsilon_1 + i\varepsilon_2$) with following relations.[36,37]

$$\epsilon_1 = 1 - \frac{\left(\gamma + n\frac{\Delta f}{f_0}\right)\frac{\Delta f}{f_0} + n\left(\frac{\Delta W}{2f_0}\right)^2}{\left(\gamma + n\frac{\Delta f}{f_0}\right)^2 + n^2\left(\frac{\Delta W}{2f_0}\right)^2} \ , \qquad (1)$$

$$\epsilon_2 = \frac{\gamma\left(\frac{\Delta W}{2f_0}\right)}{\left(\gamma + n\frac{\Delta f}{f_0}\right)^2 + n^2\left(\frac{\Delta W}{2f_0}\right)^2} \ . \qquad (2)$$

Here n denotes a depolarization factor depending on sample shape. We assume that the present shape is a prolate spheroid. A filling factor is given as $\gamma = 2.09V_s/V_0$, where V_s and V_0 represent a volume of sample and cavity, respectively. A complex conductivity ($\sigma = \sigma_1 + i\sigma_2$) is obtained by a relation of $\varepsilon = 1 + 2i\sigma/f$.

Under the identical conditions of relative humidity and Xe partial pressure at 294 K, the measurement of f_0 and W_0 are followed by one of f_s and W_s. When the relative humidity is rapidly reduced from initial 80%RH to target 20 or 50%RH, we need to readjust the sweeping frequency range, because the resonance frequency shifts from the initial range. For the adjustment, it takes about 3 min. at least. Similarly, whenever Xe pressure is applied, the sweeping frequency range has to be readjusted in the same way. The measurement on the fast process in $\sigma(t)$ mentioned later is a delicate task.

2.4 Infrared spectroscopy

Infrared absorption spectra are measured by a FT-IR spectrometer (FT/IR-6100, JASCO, Japan) combined with a pressure cell (SYJ-0126-BOD, S.T. Japan, Japan), in which relative humidity and Xe partial pressure are controlled. A Cu plate (0.5 mm thick) with an aperture of 6 mm in diameter is stuck on a Si substrate (ϕ 10 mm, and 1 mm thick). Many small samples

completely fill the aperture without light leaks. The sample substrate is set in the pressure cell, and the infrared absorption is measured for transmission configuration at 294 K. Firstly, the relative humidity is kept for 50%RH at atmospheric pressure (0 MPa). After 24 h, we measure the absorbance spectrum. Secondary, we close the valves of relative humidity control, and the pressure cell is retained for 50%RH. Then Xe pressure is applied at 0.1 MPa. After 24 h, the absorbance spectrum is measured. In the similar way, the absorbance spectra are observed up to 0.4 MPa every 0.1 MPa. In the absorbance spectra, we exclude the contribution of framework vibrations that are obtained for the measurement under vacuum.

2.5 ^{129}Xe-NMR spectrum

A ^{129}Xe-NMR experiment is generally useful to examine a structure and property of porous materials.[38] The NMR spectrum is measured with a commercial spectrometer (CMX300 model 300 MHz, Chemagnetics, USA). From the chemical shift,[39] we are available not only to identify Xe molecules embedded in the nanochannel, but also to determine the Xe partial pressure in a glass tube (ϕ 4 mm) made of Pyrex glass. The single crystals with the total weight of about 10 mg are installed at the bottom of glass tube, in which the relative humidity is 50%RH. The tube is cooled down to liquid-N_2 temperature. In order to obtain the pressure of 0.4 MPa, adequate amount of Xe gas is introduced in the tube, and then we seal it. As we gradually increase the tube temperature up to 294 K, the sample environment is pressurized. The ^{129}Xe-NMR spectrum is measured at the resonance frequency of 83.104 MHz. We use single pulse method irradiating the exposure time at 5 μs, and accumulate the spectrum at 1024 times with an interval of 0.3 s.

3. RESULTS AND DISCUSSION

3.1 Transport of the inner water molecule through WNT.

Figure 3(a) depicts the microwave conductivity of WNT constructed with H_2O (blue circles) and D_2O (red circles, D-WNT) for 80%RH. At 270 K, the conductivity in WNT is about 0.021 $(\Omega cm)^{-1}$ larger than 0.015 $(\Omega cm)^{-1}$ in D-WNT. Those are comparable values in the nanochannel water of $\{M^{III}\{H_2bim\}_3(TMA)\cdot 20H_2O\}_n$ (M = Co, Ru, Rh).[21,22] The conductivity ratio of WNT to D-WNT is almost 1.4 reflecting an isotope effect due to quasi-one-dimensional proton conduction. From the fitting (black lines), those activation energies are approximated as 0.3 eV.

Employing the TG apparatus, the amount of H_2O in the nanochannel is obtained at 294 K as a function of relative humidity in Figure 3(b), where the left vertical axis denotes the rate of weight change against 90%RH, and the right one the number of H_2O per cage length. The structure of WNT is retained for 50%RH. The $10H_2O$ molecules per cage are enclosed in WNT

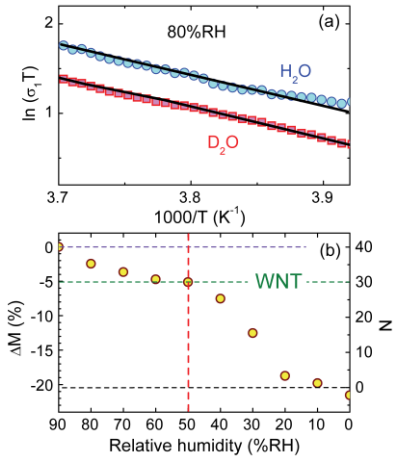

Figure 3. (a) Microwave conductivity for 80%RH in WNT composed of H_2O (blue circles) and D_2O (red squares). (b) Weight change of the single crystal with respect to relative humidity.

for 90%RH. We suspect that further H_2O is involved for 100%RH. It should be noticed that Figure 3(a) represents the proton conductivity for WNT with 5 inner water molecules per cage.

To elucidate how the inner H_2O exhibits different conducting properties from WNT, we have examined the proton conductivity for 20, 50 and 80%RH at 294 K. In Figure 4(a), relative humidity of the sample (1.50 mm in length) in the cavity is immediately changed at $t = 0$ from 80 to 20%RH, which is preserved at $t > 0$. The proton conductivity is reduced to 1 x 10^{-3} $(\Omega cm)^{-1}$ at 1 h, after that it approaches to 0 $(\Omega cm)^{-1}$. The conducting pass of proton disappears by the exclusion of almost all the hydration shells. When the sample (1.06 mm in length) is kept for 50%RH at $t > 0$ (Figure 4(b)), the conductivity at $t > 15$ h saturates to about 1 x 10^{-2} $(\Omega cm)^{-1}$, indicating that the proton is transferable by way of WNT.

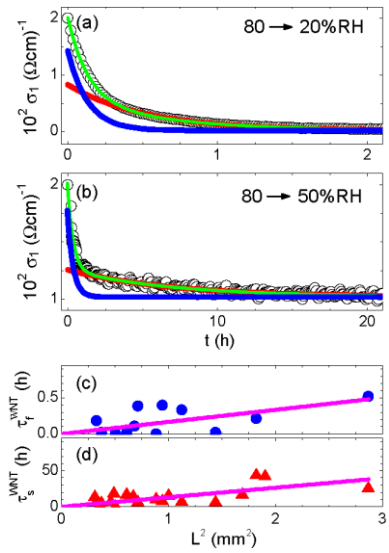

Figure 4. (a, b) Time variation of the conductivity after relative humidity was rapidly changed at $t = 0$ from 80 to 20%RH, and to 50%RH. (c, d) Relaxation times in the fast and slow processes (τ_f^{WNT} and τ_s^{WNT}) *vs.* L^2 for 50%RH.

The proton conductivity in Figures 4(a) and 4(b) is reproduced with following exponential curves due to fast and slow processes,

$$\sigma_1(t) = \sigma_0(x) + \sigma_f(x) \exp(-t/\tau_f^{WNT}(x)) + \sigma_s(x) \exp(-t/\tau_s^{WNT}(x)). \quad (3)$$

The conductivity in Figure 4(a) is fitted with the green curve that is a sum of blue curve (σ_0(20%RH) ~ 0, σ_f(20%RH) = 0.014 $(\Omega cm)^{-1}$ and τ_f^{WNT}(20%RH) = 0.13 h) and red curve (σ_s(20%RH) = 0.0059 $(\Omega cm)^{-1}$ and τ_s^{WNT}(20%RH) = 0.61 h). Similarly, in Figure 4(b), the fitting parameters are determined as σ_0(50%RH) ~ 0.01, σ_f(50%RH) = 0.007, σ_s(50%RH) = 0.0024 $(\Omega cm)^{-1}$, τ_f^{WNT}(50%RH) = 0.37 and τ_s^{WNT}(50%RH) = 7.0 h. Although τ_f^{WNT}(50%RH) is about twice as large as τ_f^{WNT}(20%RH), τ_s^{WNT}(50%RH) is one order of magnitude larger than τ_s^{WNT}(20%RH). In the non-equilibrium state at $t > 0$, the inner H_2O, which diffuses quasi one-dimensionally in WNT, is exhausted from the sample edge. In the dehydrated process, WNT plays a role of nanofluidic channel.

A one-dimensional diffusion is described by Fick's second law, the solution of which provides a time variation of concentration of diffusing substance.[40] The variation of σ_1 is associated with the concentration change of the inner water molecules. If the conductivity is proportional to the concentration of inner H_2O, the time variation is given by the following term in the solution.

$$\sigma_i(t) \propto \exp\left(-\frac{(2n+1)^2\pi^2}{L^2} D_i^{WNT} t\right) \quad (i = f, s). \quad (4)$$

Here L and D_i^{WNT} are sample length and diffusion constant, respectively. The lowest term ($n = 0$) makes dominant contribution, so that we can neglect the higher order ones ($n > 0$). Two different diffusion constants are introduced to explain the fast (f) and slow (s) processes. From eqs. (3) and (4), the relaxation time is related to the diffusion constant as follows.

$$\tau_i^{WNT}(x) = L^2 / \pi^2 D_i^{WNT}(x) \quad (i = f, s). \quad (5)$$

For many samples with different lengths, we have measured and analyzed the time variation of conductivity for 80→50%RH as well. In Figures 4(c) and 4(d), τ_f^{WNT}(50%RH) and τ_s^{WNT}(50%RH) as a function of L^2 are well reproduced by the least-square fitted lines (pink lines). Those results support that the time-variation of conductivity is dominated by the concentration of inner H_2O.

From the fitted lines in Figures 4(c) and 4(d), the translational diffusion constants of fast and slow processes are estimated as D_f^{WNT}(50%RH) = 2 x 10^{-10} and D_s^{WNT}(50%RH) = 2 x 10^{-12} m^2/s, respectively. Viscosity of the inner H_2O is expected to depend on the hydration strength inside of WNT.[41] The fast diffusion may arise from H_2O molecules occupying at the central area of nanochannel with the weakest interfacial interaction, and the slow one is attributable to H_2O molecules hydrogen bonding to WNT.

3.2 Storage of Xe in WNT.

Xe partial pressures of 0.1 (Figure 5(a)) and 0.4 MPa (Figure 5(b)) are applied to the saturated samples for 50%RH with the lengths of 1.06 and 0.97 mm, respectively. In those figures, t = 0 is redefined as the time when the pressure is applied. The time variation of proton conductivity, which rapidly drops and gradually approaches to zero (σ_0(0.1 MPa) = σ_0(0.4 MPa) ~ 0), is reproducible with eq. (3) as well. In Figure 5(a), the data is fitted by a green curve, which is a sum of fast process (blue curve) with σ_f(0.1 MPa) = 0.0027 $(\Omega cm)^{-1}$ and τ_f^{Xe}(0.1 MPa) = 0.33 h, and slow one (red curve) with σ_s(0.1 MPa) = 0.0065 $(\Omega cm)^{-1}$ and τ_s^{Xe}(0.1 MPa) = 43 h. Similarly, the conductivity in Figure 5(b) is decomposed into the fast process (σ_f(0.4 MPa) = 0.0064 $(\Omega cm)^{-1}$ and τ_f^{Xe}(0.4 MPa) = 0.17 h), and the slow one (σ_s(0.4 MPa) = 0.0033 $(\Omega cm)^{-1}$ and τ_s^{Xe}(0.4 MPa) = 6.3 h). Although τ_f^{Xe}(0.1 MPa) is a factor of two large compared to τ_f^{Xe}(0.4

MPa), τ_s^{Xe}(0.1 MPa) is one-order of magnitude greater than τ_s^{Xe}(0.4 MPa). Employing the several samples with different lengths, we also measured the conductivity at 0.4 MPa. In Figures 5(c) and 5(d), τ_f^{Xe}(0.4 MPa) and τ_s^{Xe}(0.4 MPa) *vs.* L^2 are well fitted with straight lines. Since the framework structure is little varied under such tiny pressures, the suppression of proton conductivity is rationalized as a consequence of the penetration of Xe in WNT.

On behalf of verifying that Xe actually resides in the nanochannel, we have measured the chemical shift for the sample pressurized by Xe in the glass tube at 294 K.[38,42] In Figure 5(e), a signal at 1.9 ppm proves that the pressure inside the tube is approximated as 0.4 MPa.[42]

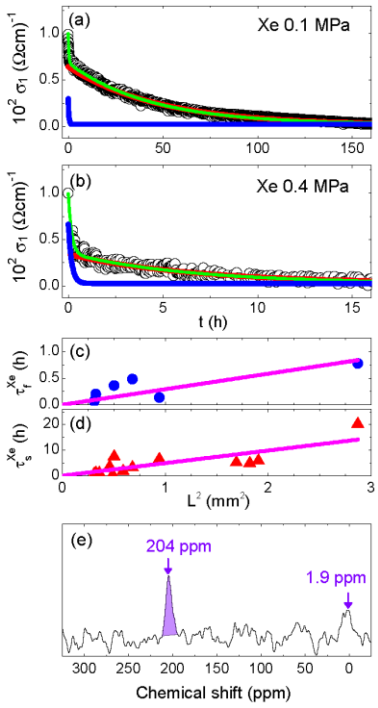

Figure 5. (a, b) Time variation of conductivity under Xe pressures of 0.1 and 0.4 MPa applied at t = 0. (c, d) Relaxation times in the fast and slow processes (τ_f^{Xe} and τ_s^{Xe}) *vs.* L^2 at 0.4 MPa. (e) Chemical shift measured at 0.4 MPa. The signal at 204 ppm ensures that Xe is encaged in WNT.

Furthermore, there appears a remarkable signal at 204 ppm, which is caused by Xe inside of WNT. Therefore the suppression of proton conductivity is associated with the increase of Xe concentration in WNT.

The absorption spectra of OH stretching vibration for 50%RH up to 0.4 MPa are shown in Figures 6(a)-6(c). The broad OH stretching band is well decomposed into three Lorentzian curves, for which the resonance frequency (*f*) and integrated absorbance (*S*) are plotted by solid symbols with the same colors in Figures 6(d) and 6(e), respectively. The resonance frequency little depends on pressure. The low-frequency band (green curves) comes from a response of H_2O molecules possessing a tetrahedral configuration, whereas the middle- and high-frequency bands are assigned as the OH stretching vibration of the fourth-hydration H_2O with free OH. The integrated absorbance of low-frequency band normalized at 0 MPa (green solid squares in Figure

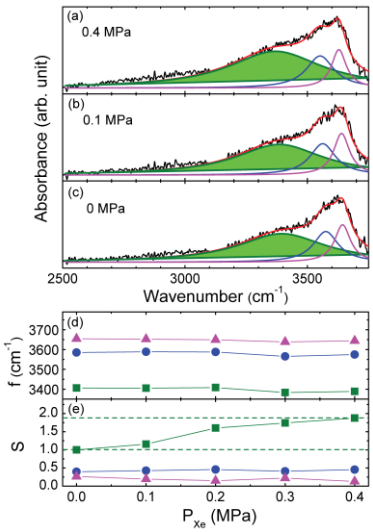

Figure 6. (a-c) Infrared absorbance spectra decomposed into three Lorentzian curves for each pressure. (d, e) Resonance frequency (*f*) and integrated absorbance (*S*) as a function of Xe partial pressure.

6(e)) tends to saturate above 0.2 MPa, while no change appears in another bands. The enlargement of *S* means that the water content increases. In addition to Xe, water molecules are found to penetrate into WNT.

From *f* for the low-frequency band, the average O-O distance is estimated as 2.8 Å,[44,45] which is larger than 2.75 Å in the water network of $\{M\{H_2bim\}_3(TMA)\cdot 20H_2O\}_n$,[22] and hence the present WNT holds a soft tendency. We have estimated the amount of H_2O in light of the integrated absorbance relevant to the number of oscillators. In Figure 6(e), the integrated absorbance of low-frequency band at 0.4 MPa is about 1.9 times as large as one at 0 MPa. The WNT except for the fourth hydration shell consists of $28H_2O$ molecules per cage length at 0 MPa. The content of nanochannel water is estimated to be about $53H_2O$ per cage length at 0.4 MPa. Therefore WNT accommodates both Xe and about 25 inner water molecules per cage. Those form a Xe hydrate, which is stabilized at low pressures compared to conventional clathrate hydrate of Xe. The time variation of conductivity in Figures 5(a) and 5(b) is regarded as a formation process of the Xe hydrate.

According to the fitted results (pink lines) in Figures 5(c) and 5(d), it is reasonable to consider that the conductivity is dominated by the concentration change ($C(t=\infty) - C(t)$) of Xe hydrate as similarly described with the translational diffusion constant of eq. (5) as follows.

$$\sigma_i \propto C_\infty - C(t) \propto \exp\left(-\frac{\pi^2}{L^2} D_i^{\mathrm{Xe}} t\right) \quad (i = \mathrm{f, s}). \qquad (6)$$

The translational diffusion constants of D_f^{Xe}(0.4 MPa) and D_s^{Xe}(0.4 MPa) are respectively evaluated as 1×10^{-10} and 6×10^{-12} m^2/s, which are comparable to the self-diffusion constants in Xe solution.[46]

The water concentration inside of WNT is estimated to be 0.23 and 0.46 g/cm^3 for 80 and 90%RH, respectively. To reach the density of ice I_h (0.92 g/cm^3) or liquid free water (1 g/cm^3),

WNT needs to encage 20 or 24H_2O molecules per cage, respectively. Those values are almost identical to 21.5H_2O molecules constructing a Xe hydrate in Xe solution,[46] which exhibits the chemical shift of 196 ppm.[47] In Figure 5(e), 204 ppm is slightly close to the signal of Xe in dodecahedral cage (5^{12}, 20H_2O) rather than tetrakaidecahedral one ($5^{12}6^2$, 24H_2O) of clathrate hydrate structure I of Xe.[48] In the present system, Xe may be encompassed with about 22H_2O among 25H_2O, and the other is expected to situate in a space between the Xe hydrate and WNT. In terms of van der Waals interactions between Xe molecules, single Xe could be involved in the cage at low pressure, and empty cages may exist.[49]

To answer a question why additional water molecules are necessarily encaged in WNT, we discuss the stability of Xe. From a Lenard-Jones potential, the repulsive van der Waals interaction between Xe and H_2O in the cyclic hexagon is evaluated to be 12.3 meV (= 143 K) that is lower than room temperature, and hence Xe could go through WNT. In clathrate hydrates, a guest molecule is capable to transfer from cage to cage by way of five- or six-membered water rings. First principle calculations have shown that the six-membered water ring is remarkably distorted by mobile CH_4 in comparison with H_2 and CO_2.[50-52] The diffusive Xe may little distort the cyclic hexagon, because D_f^{Xe}(0.4 MPa) and D_s^{Xe}(0.4 MPa) is about three orders of magnitude larger than the self-diffusion constant of CO_2 at high pressure (10^{-13}-10^{-14} m^2/s).[53]

In noble gas hydrates, host-guest and guest-guest interactions are strongly dependent on the size of guest species.[54] A force attracting between H_2O and Xe is obtained by differentiating the Lenard-Jones potential with respect to the distance. The equilibrium distance is evaluated as 3.8 Å, which is consistent with O-Xe distance of 3.84 Å obtained by the ab initio calculation in a dodecahedral cage.[55] An independent Xe molecule is unstable in WNT, because the equilibrium distance is about 30% smaller than the radius of present water cage (~ 5 Å). Additional water

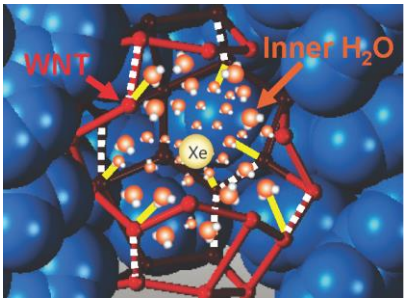

Figure 7. Schematic illustration of Xe surrounded by H_2O molecules in WNT. White dotted lines indicate that the original hydrogen bond in WNT is broken owing to the formation of hydrogen bonds between inner H_2O and WNT (yellow lines).

molecules are required to fill the gap for the stabilization.

Despite the plenty of inner H_2O molecules, the conductivity approaches to 0 $(\Omega cm)^{-1}$ in contrast to ~0.02 $(\Omega cm)^{-1}$ for 80%RH in Figure 4. The host-guest (H_2O-Xe) interaction is expected to harden the whole hydrogen-bonding water network in addition to the interfacial interaction from the framework. On the analogy of the water network of $\{M\{H_2bim\}_3(TMA)\cdot 20H_2O\}_n$,[22] Eigen-type hydrates ($H_3O^+(H_2O)_3$) are considered to contribute to the proton conduction. A proton transfer from H_3O^+ to adjacent H_2O is accompanied by a local distortion of O-O distance. Since the hardening of the water network prevents such distortions, the transfer rate of proton may be suppressed.

The forth hydration shell makes little contribution for the hydrogen bond to the Xe hydrate, because there is no change in the middle and high absorption bands in Figures 6(a)-6(c). For the stabilization of Xe hydrate, the H_2O surrounding Xe needs to be anchored to the primary, secondary or tertiary hydration shells of WNT. In order to make the coupling between them, some of the original hydrogen bonds in those shells have to be broken (dotted white lines) and

rearranged (yellow lines) as schematically illustrated in Figure 7. In this situation, WNT itself may be greatly altered in structure. The reorganization of hydrogen bonds is considered to block the proton-conducting pass parallel to the nanochannel. Both the hardening and reorganization may contribute to the suppression of proton conduction.

4. CONCLUSIONS

From the isotope effect in the microwave conductivity for 80%RH, WNT confined in the insulating nanochannel is found to be a quasi-one-dimensional proton conductor. The change of sample weight as a function of relative humidity makes clear that the structure of WNT is retained for 50%RH, above which the inner H_2O molecules exist. According to the exponential time variation of proton conductivity for 80→50%RH under atmospheric pressure, the diffusion of the inner H_2O is characterized by the fast and slow processes by way of WNT that plays a role of nanofluidic channel. Upon pressurizing Xe at 0.1 and 0.4 MPa for 50%RH, the proton conductivity exhibits the exponential time variation that is also divided into the fast and slow processes. Those translational diffusion times are comparable to self-diffusion times in Xe solution. In the ^{129}Xe-NMR experiment at 0.4 MPa, the chemical shift detected at 204 ppm proves that Xe is embedded in WNT. Furthermore, the OH stretching band at 0.4 MPa reveals that about 25H_2O molecules exist in the cage. Those experimental results demonstrate that the Xe hydrate in WNT inhibits the proton conduction. The inhibition may be related to the hardening and reorganization of the hydrogen-bonding water network.

Figure 5(a) shows that the Xe hydrate is stabilized in WNT even at 0.1 MPa. If soluble Xe enters into a nervous system involving lots of H_2O molecules, Xe hydrates could be easily formed in the confined geometry. In light of the present results, it is highly probable that Xe

hydrates inhibit a neural transmission in Xe-inhalation anesthesia. Finally, we should remind that Xe is stabilized in WNT at low pressures compared to the conventional clathrate hydrate. Nanochannel water has great potential of gas storage and transportation under mild conditions.

AUTHOR INFORMATION

Corresponding Author

*E-mail: hiroshi.matsui.b2@tohoku.ac.jp

ORCID

Hiroshi Matsui: 0000-0002-7402-0755

Makoto Tadokoro: 0000-0002-0049-7606

Author Contributions

H. M., T. S., and M. T. contributed equally to this work.

Notes

The authors declare no competing financial interest.

ACKNOWLEDGEMENTS

This work was supported by JSPS KAKENHI Grant Numbers 24340071, 24651127, 15H03851, and 17K05825. The authors would like to thank J. Sakuma for his help in experiments.

REFERENCES

(1) Kreuer, K. D.; Paddison, S. J.; Spohr, E.; Schuster, M. Transport in Proton Conductors for Fuel-Cell Applications: Simulations, Elementary Reactions, and Phenomenology. *Chem. Rev.* **2004**, *104*, 4637-4678.

(2) Elimelech, M.; Phillip, W. A. The Future of Seawater Desalination: Energy, Technology, and the Environment. *Science* **2011**, *333*, 712-717.

(3) Zao, K.; Wu, H. Fast Water Thermo-pumping Flow across Nanotube Membranes for Desalination. *Nano Lett.* **2015**, *18*, 3664-3668.

(4) Zhong, C.; Deng, Y.; Roudsari, A. F.; Kapetanovic, A.; Anantrm, M. P.; Rolandi, M. A Polysaccharide Bioprotonic Field-Effect Transistor. *Nat. Commun*. **2011**, *2*, 476.

(5) Guo, L.; Wen, J.; Ding, J.; Wan, C.; Cheng, G. Excitatory Post-Synaptic Potential Mimicked in Indium-Zinc-Oxide Synaptic Transistors Gated by Methyl Cellulose Solid Electrolyte. *Sci. Rep*. **2016**, *6*, 38578.

(6) Feng, P.; Du, P.; Wang, C.; Shi, Y.; Wan, Q. Proton Conducting Graphene Oxide/Chitosan Composite Electrolytes as Gate Dielectrics for New-Concept Devices. *Sci. Rep*. **2016**, *6*, 34065.

(7) Wu, G.; Feng, P.; Wan, X.; Zhu, L.; Shi, Y.; Wan, Q. Artificial Synaptic Devices Based on Natural Chicken Albumen Coupled Electric-Double-Layer Transistors. *Sci. Rep*. **2016**, *6*, 23578.

(8) Matsuo, Y.; Ikeda, H.; Kawabata, T.; Hatori, J.; Oyama, H. Collagen-Based Fuel Cell and Its Proton Transfer. *Mater. Sci. Appl*. **2017**, *8*, 747-756.

(9) Daiguji, H. Ion Transport in Nanofluidic Channels. *Chem. Soc. Rev*. **2010**, *39*, 901-911.

(10) Shao, J. J.; Raidongia, K.; Koltonow, A. R.; Huang, J. Self-Assembled Two-Dimensional Nanofluidic Proton Channels with High Thermal Stability. *Nat. Commun*. **2015**, *6*, 7602.

(11) Trigg, E. B.; Gaines, T. W.; Maréchal, M.; Moed, D. E.; Rannou, P.; Wagener, K. B.; Stevens, M. J.; Winey, K. I. Self-Assembled Highly Ordered Acid Layers in Precisely Sulfonated Polyethylene Produce Efficient Proton Transport. *Nat. Mater*. **2018**, *17*, 725-731.

(12) Zhang, Z.; Kashiwagi, H.; Kimura, S.; Kong, S.; Ohta, Y.; Miyake, T. A Protonic Biotransducer Controlling Mitochondrial ATP Synthesis. *Sci. Rep*. **2018**, *8*, 10423.

(13) Maniwa, Y.; Kataura, H.; Abe, M.; Udaka, A.; Suzuki, S.; Achiba, Y.; Kira, H.; Matsuda, K.; Okabe, Y. Ordered Water inside Carbon Nanotubes: Formation of Pentagonal to Octagonal Ice-Nanotubes. *Chem. Phys. Lett*. **2005**, *401*, 534-538.

(14) Yang, Y.; Li, X.; Jiang, J.; Du, H.; Zao, L.; Zao, Y. Control Performance and Biomembrane Disturbance of Carbon Nanotube Artificial Water Channels by Nitrogen-Doping. *ACS Nano* **2010**, *4*, 5755-5762.

(15) Falk, K.; Sedlmeier, F.; Joly, L.; Netz, R. R.; Bocquet, L. Molecular Origin of Fast Water transport in Carbon Nanotube Membranes: Superlubricity versus Curvature Dependent Friction. *Nano Lett.* **2010**, *10*, 4067-4073.

(16) Kou, J.; Lu, H.; Wu, F.; Fan, J.; Yao, J. Electricity Resonance-Induced Fast Transport of Water through Nanochannels. *Nano Lett.* **2014**, *14*, 4931-4936.

(17) Parlak, O.; Keene, S. T.; Marais, A.; Curto, V. F.; Salleo, A. Molecularly Selective Nanoporous Membrane-Based Wearable Organic Electrochemical Device for Noninvasive Cortisol Sensing. *Sci. Adv*. **2018**, *4*, 2904.

(18) Chen, X.; Plonka, A. M.; Banerjee, D.; Krishna, R.; Schaef, H. T.; Ghose, S.; Thallapally, P. K.; Parise, J. B. Direct Observation of Xe and Kr Adsorption in a Xe-Selective Microporous Metal-Organic Framework. *J. Am. Chem. Soc*. **2015**, *137*, 7007-7010.

(19) Mason, J. A.; Oktawiec, J.; Taylor, M. K.; Hudson, M. R.; Rodriguez, J.; Bachman, J. E.; Gonzalez, M. I.; Cervellino, A.; Guagliardi, A.; Brown, C. M.; et al. Methane Storage in Flexible Metal-Organic Frameworks with Intrinsic Thermal Management. *Nature* **2015**, 527, 357-361.

(20) Banerjee, D.; Simon, C. M.; Plonka, A. M.; Motkuri, R. K.; Liu, J.; Chen, X.; Smit, B.; Parise, J. B.; Haranczyk, M.; Thallapally, P. K. Metal-Organic Framework with Optimally Selective Xenon Adsorption and Separation. *Nature Comm*. **2016**, *7*, 11831.

(21) Matsui, H.; Ohhata, Y.; Iida, C.; Horii, M.; Tadokoro, M. Observation of Quasi-One Dimensional Proton Conductions in Molecular Porous Crystal $[Co^{III}(H_2bim)_3](TMA)\cdot 20H_2O$. *J. Phys. Soc. Jpn.* **2010**, *79*, 103601.

(22) Matsui, H.; Tadokoro, M. Eigen-like Hydrated Protons Travelling with a Local Distortion through the Water Nanotube in New Molecular Porous Crystals $\{[M^{III}(H_2bim)_3](TMA)\cdot 20H_2O\}_n$ (*M* = Co, Rh, Ru). *J. Chem. Phys*. **2012**, *137*, 144503.

(23) Matsui, M.; Suzuki, Y.; Fukumochi, H.; Tadokoro, M. Defect Dynamics of the Dipole Ordered Water Chain in a Polar Nanochannel. *J. Phys. Soc. Jpn*. **2014**, *83*, 054708.

(24) Matsui, H.; Tadokoro, M. Proton Conduction through the Nanochannel Water in Weak-Acidic Nanoporous Crystals $[Cu_2(phen)_2(AcO)_2(H_2O)_2][Al(OH)_6Mo_6O_{18}]M^+(nH_2O)$ ($M^+ = H^+, Li^+, Na^+, K^+$). *Solid State Ionics* **2016**, *285*, 165-169.

(25) Xu, H.; Tao, S.; Jiang, D. Proton Conduction in Crystalline and Porous Covalent Organic Frameworks. *Nat. Mater*. **152016**, 15, 4611.

(26) Liu, M. ; Chen, L.; Lewis, S.; Chong, S. Y.; Little, M. A.; Hasell, T.; Aldous, I. M.; Brown, C. M.; Smith, M. W.; Morrison, C. A.; et al. Three-Dimensional Protonic Conductivity in Porous Organic Cage Solids. *Nat. Commun*. **2016**, *7*, 12750.

(27) Sloan, E. D.; Koh, C. A. *Clathrate Hydrates of natural Gases 3rd ed.*, CRC Press: Boca Raton, 2008.

(28) Ohgaki, K.; Sugihara, T.; Suzuki, M.; Jindai, H. Phase Behavior of Xenon Hydrate System. *Fluid Phase Equilibria* **2000**, *175*, 1-6.

(29) Isidoro, R. P.; Valdez, F. J. S.; Suarez, J. C. R. Anesthetic Diffusion through Lipid Membranes Depends on the Protonation Rate. *Sci. Rep*. **2014**, *4*, 7534.

(30) Valdez, F. J. S.; Suarez, J. C. R. Noble Gases in Pure Lipid Membranes. *J. Phys. Chem. B*

2013, *117*, 3167-3172.

(31) Pauling, L.; A Molecular Theory of General Anesthesia. *Science* **1961**, *134*, 15-21.

(32) Garczarek, F.; Gerwert, K. Functional Waters in Intraprotein Proton Transfer Monitored by FTIR Difference Spectroscopy. *Nature* **2006**, *439*, 109-112.

(33) Tadokoro, M.; Iida, C.; Shimazaki, Y.; Isoda, K.; Suzuki, Y.; Sugaya, T.; Kumagai, Y.; Mizuno, M. Water Nanotubes Clathrating Solvent Molecules Stabilized by Molecular 1-D Nanoporous Crystals. *RSC Advances* **2012**, *2*, 12101-12104.

(34) Tadokoro, M.; Iida, C.; Saito, T.; Suda, T.; Miyazato, Y. One-Dimensional Tube-Like $\{5^{12}6^{2}\}_{n}$ Water Clusters Stabilized in a Molecular Nanoporous Framework. *Chem. Lett.* **2010**, *39*, 186-187.

(35) Öhrström, L.; Larsson, K. What Kinds of Three-Dimensional Nets Are Possible with Tris-Chelated Metal Complexes as Building Blocks? *Dalton trans.* **2004**, 347-353.

(36) Klein, O.; Donovan, S.; Dressel, M.; Grüner, G. Microwave Cavity Perturbation Technique: Part I: Principles. *Int. J. Infrared and Millimeter Waves* **1993**, *14*, 2423-2457.

(37) Dressel, M.; Klein, O.; Donovan, S.; Grüner, G. Microwave Cavity Perturbation Technique: Part III: Applications. *Int. J. Infrared and Millimeter Waves* **1993**, *14*, 2489-2517.

(38) Weiland, E.; Huet, M. A. S.; Nossov, A.; Gedeon, A. ^{129}Xe NMR: Review of Recent Insights into Porous Materials. *Microporous Mesoporous Mater*. **2016**, *225*, 41-65.

(39) Jameson, C. J.; Jameson, A. K.; Cohen, S. M. Temperature and Density Dependence of ^{129}Xe Chemical Shift in Xenon Gas. *J. Chem. Phys*. **1973**, *59*, 4540-4546.

(40) Crank, J. *The mathematics of diffusion 2nd ed*.; Oxford University Press: London, U.K., 1975.

(41) Wu, K.; Chen, Z.; Xiangfang, J. L.; Xu, J.; Dong, X. Wettability Effect on Nanoconfined

Water Flow. *Proc. Natl. Acad. Sci. USA* **2017**, *114*, 3358-3363.

(42) Brouwer, D. H.; Alavi, A.; Ripeester, J. A. A Double Quantum ^{129}Xe NMR Experiment for Probing Xenon in Multiply-Occupied Cavities of Solid-State Inclusion Compounds. *Phys. Chem. Chem. Phys*. **2007**, *9*, 1093-1098.

(43) Haake, M.; Goodson, B. M.; Laws, D. D.; Brunner, E.; Cyrier, M. C.; Havlin, R. H.; Pines, A. NMR of Supercritical Laser-Polarized Xenon. *Chem. Phys. Lett*. **1998**, *292*, 686-690.

(44) Novak, A. In *Structure and Bonding*; Dunitz, J. D.; Hemmerich, P.; Holm, R. H.; Ibers, J. A.; Jorgensen, C. K.; Neilands, J. B.; Reinen, D.; Williams, R. J. P., Eds.; Springer-Verlag, New York, 1974; Vol. 18, pp 177-216.

(45) Maréchal, Y. *The Hydrogen Bond and the Water Molecule*; Elsevier: Amsterdam, Netherland, 2007.

(46) Artyukhov, V. I.; Pulver, A. Y.; Peregudov, A.; Artyuhov, I. Can Xenon in Water Inhibit Ice Growth? Molecular Dynamics of Phase Transitions in Water-Xe System. *J. Chem. Phys*. **2014**, *141*, 034503.

(47) Jameson, C. J.; Sears, D. N.; Murad, S. Molecular Dynamics Averaging of Xe Chemical Shifts in Liquids. *J. Chem. Phys*. **2004**, *121*, 9581-9592.

(48) Jameson, C. J.; Stueber, D. The Nuclear Magnetic Resonance Line Shapes of Xe in the Cages of Clathrate Hydrates. *J. Chem. Phys*. **2004**, *120*, 10200-10214.

(49) Fukazawa, T. I.; Yamaguchi, Y.; Nagashima, K.; Kawamura, K. Structure and Dynamics of Empty Cages in Xenon Clathrate Hydrate. *J. Chem. Phys*. **2008**, *129*, 224506.

(50) Pérez, G. R.; Moaied, M.; Soler, J. M.; Yndurain, F. Stability, Adsorption, and Diffusion of CH_4, CO_2, and H_2 in Clathrate Hydrates. *Phys. Rev. Lett*. **2010**, *105*, 145901.

(51) Vidal, Á. V.; Rodríguez, M. P.; Pinerio, M. M. Direct Transition Mechanism for Molecular

Diffusion in Gas Hydrates. *RSC Advances* **2016**, *6*, 1966-1972.

(52) Ranieri, U.; Koza, M. M.; Kuhs, W. F.; Klotz, S.; Falenty, A.; Gillet, P.; Bove, L. E. Fast Methane Diffusion at the Interface of Two Clathrate Structures. *Nat. Commun*. **2017**, *8*, 1076.

(53) Liang, S.; Liang, D.; Wu, N.; Yi, L.; Hu, G. Molecular Mechanisms of Gas Diffusion in CO_2 Hydrates. *J. Phys. Chem. C* **2016**, *120*, 16298-16304.

(54) Kaur, S. P.; Ramachandran, C. N. Host-Guest and Guest-Guest Interactions in Noble Gas Hydrates. *Mol. Phys*. **2018**, *116*, 54-63.

(55) Kumar, P.; Sathyamurthy, N. Theoretical Studies of Host-Guest Interaction in Gas Hydrates. *J. Phys. Chem. A* **2011**, *115*, 14276-14281.